catalysts

MDPI

Article

Enhanced Cyclopentanone Yield from Furfural Hydrogenation: Promotional Effect of Surface Silanols on Ni-Cu/m-Silica Catalyst

Ravi Balaga [1,2,3,4], Putrakumar Balla [5], Xiaoqiang Zhang [1,2,3], Kishore Ramineni [6], Hong Du [1,2,3], Shrutika Lingalwar [4], Vijayanand Perupogu [4] and Zongchao Conrad Zhang [1,2,*]

1 State Key Laboratory of Catalysis, Dalian Institute of Chemical Physics, Chinese Academy of Sciences, Dalian 116023, China
2 Dalian National Laboratory for Clean Energy, Dalian Institute of Chemical Physics, Chinese Academy of Sciences, Dalian 116023, China
3 University of Chinese Academy of Sciences, Beijing 100049, China
4 Energy & Environmental Engineering Department CSIR-Indian, Institute of Chemical Technology, Hyderabad 500007, Telangana, India
5 Department of Chemical Engineering and Applied Chemistry, Chungnam National University, Daejeon 34134, Republic of Korea
6 Department of Chemistry, Anurag University, Hyderabad 500088, Telangana, India
* Correspondence: zczhang@yahoo.com

Abstract: A direct alkaline hydrothermal method was used to synthesize mono- and bimetallic Ni and Cu on mesoporous silica (m-SiO_2) as catalysts for the hydrogenation of furfural (FAL) to cyclopentanone (CPO). The catalysts were characterized by XRD, FTIR, H_2-TPR, SEM, TEM, HR-TEM, XPS, ICP, BET, and CHN analysis. The results demonstrate that the addition of Cu metal improved the reducibility of Ni catalysts and revealed Ni-Cu alloy formation over m-SiO_2. Furthermore, XPS and FTIR results reveal that the silanol groups on the catalyst surface play an important role in the ring rearrangement of furfuryl alcohol. Hence, the effect of silanol groups in the FOL rearrangement was studied in detail. Among the catalysts at fixed metal loading of 20 wt.%, Ni_5Cu_{15}/m-SiO_2 catalyzed the formation of CPO as the main product due to the synergy of Ni-Cu alloy and surface silanol groups. Ni_5Cu_{15} supported on a commercial mesoporous silica (Ni_5Cu_{15}/C-SiO_2) showed inferior performance compared with the Ni_5Cu_{15}/m-SiO_2 catalyst for the FAL hydrogenation. Reaction temperature and time were also optimized for the enhanced CPO yield over Ni_5Cu_{15}/m-SiO_2. The Ni_5Cu_{15}/m-SiO_2 catalyst is durable, as demonstrated by stability tests over multiple reuses. This effective and flexible Ni_xCu_y on m-SiO_2 catalyst provides an effective candidate for efficient upgrading of furanics in selective hydrogenation reactions.

Keywords: biomass; hydrogenation; furfural; cyclopentanone; Ni-Cu alloy; surface silanols

Citation: Balaga, R.; Balla, P.; Zhang, X.; Ramineni, K.; Du, H.; Lingalwar, S.; Perupogu, V.; Zhang, Z.C. Enhanced Cyclopentanone Yield from Furfural Hydrogenation: Promotional Effect of Surface Silanols on Ni-Cu/m-Silica Catalyst. *Catalysts* **2023**, *13*, 580. https://doi.org/10.3390/catal13030580

Academic Editor: Federica Menegazzo

Received: 12 February 2023
Revised: 5 March 2023
Accepted: 10 March 2023
Published: 13 March 2023

1. Introduction

Producing biofuels and biochemicals from cellulosic biomass feedstock is a green approach to address the energy and environmental challenges associated with the large consumption of fossil resources [1]. Furfural (FAL), the most abundant platform chemical derived from hemicellulose, can be transformed into a number of valuable compounds, including furfuryl alcohol (FOL), 2-methylfuran (2-MF), α, ω-pentanediol(PeD), cyclopentanone (CPO), and cyclopentanol (CPL) [2–5]. Of particular importance, CPO is a high-value chemical intermediate for synthesizing perfumes, cosmetic goods, and agrochemicals [6]. Industrially, CPO is produced from intramolecular decarboxylation of adipic acid or sequential hydration and dehydrogenation of cyclopentene [7]. Adipic acid mainly comes from non-renewable fossil resources through multistep synthesis, generating significant waste streams during the process [8]. Sequential hydration and dehydrogenation of cyclopentene

to CPO requires a noble metal catalyst operating at high temperatures (280–300 °C) and high pressures (25–40 MPa) [9].

Recently, biomass-based furfural was shown to be a suitable feedstock to produce CPO in aqueous medium. Hronec et al. first reported 81.3% overall yield of CPO and CPL by using 5% of Pt/C catalyst at 160 °C and 8 MPa H_2 pressure [10]. Other precious metal catalysts (Au, Ru, Rh, and Pt) have also been widely studied in this reaction with excellent catalytic performances [9]. However, the processes carry the cost associated with the noble metals [11–13]. Recently, non-noble metal catalysts such as Cu, Co, Fe, and Ni have been reported to be active catalysts for the hydrogenation of FAL with promising catalytic activity [9]. In addition, it has been reported that bimetallic catalysts performed better than monometallic catalysts and showed high selectivity and activity for the hydrogenation of FAL to CPO in the aqueous phase through the formation of alloys [14–16]. Li et al. reported that a Ni-Co/TiO_2 catalyst with 10 wt.% of Co and 10 wt.% of Ni showed a CPO productivity of 2.3 mmol $g_{cat}{}^{-1}$ h^{-1} with 53.3% selectivity to CPO [15]. However, the catalyst was deactivated due to the leaching of active metals in water medium. Later, Xu et al. reported that a Ni-Cu/SBA–15 catalyst with an equal molar of Cu and Ni showed a CPO productivity of 5.8 mmol $g_{cat}{}^{-1}$ h^{-1} with 62% selectivity to CPO, where three key intermediates, furfuryl alcohol (FOL), 4-hydroxy-2-cyclopentenone (4-HCP) and 2-cyclopentenone (2-CPEO), were identified [17]. In another study, Xu et al. reported the CPO productivity of 6.3 mmol $g_{cat}{}^{-1}$ h^{-1} with 83.6% selectivity to CPO using a Ni-Cu/Al-MCM-41 catalyst [18]. It was proposed that the formation of Ni-Cu alloy may suppress the hydrogenation of C=C bonds in the furan ring of furfural and the sintering of Cu species in an aqueous medium. The acid sites appear to play an essential role in the formation of CPO by rearrangement of FOL. Sitthisa et al. [19] reported that FAL mainly interacted with silanol groups through hydrogen bonding. The weak acid associated with the silanol groups on the surface of silica has been reported as the active sites in Beckmann rearrangement and cumene cracking [20,21]. Sun et al. [22] reported that *in situ* synthesized Fe and Co on silica by direct alkaline hydrothermal method contain silanol groups after doping the metals. In the earlier works, the in situ incorporation of metal ions (Ni, Cu, Co, and co-metals) into the tetrahedral framework positions of the siliceous material was successfully achieved and applied in various applications such as catalytic reduction of 4-nitrophenol, conversion of methane to syngas, carbon dioxide reforming, etc. [23–26]. The in situ prepared catalysts have shown high catalytic activity and stability due to the dispersion of active sites on silica matrices [22,27]. We also found that the in situ prepared catalysts exhibited excellent catalytic performance in the hydrogenation of FAL to THFA in water solvent [28].

Inspired by the above works, we prepared Ni_xCu_y uniformly distributed in silica matrix by using an in situ direct alkaline hydrothermal method, specifically for the hydrogenation of FAL to CPO through the formation of Ni-Cu alloy with the presence of abundant surface silanol groups. In this study, the monometallic Cu, Ni, and bimetallic Ni-Cu on m-SiO_2 catalysts were investigated for their catalytic activities. XRD, H_2–TPR, SEM, XPS, FTIR, and HR-TEM were used to investigate the Ni-Cu interaction and the effect of silanol groups on the silica surface. In comparison, a catalyst with the same metal loading was prepared by the wet impregnation method and studied for FAL hydrogenation. The conversion of FAL and the selectivity of CPO were optimized over temperature and time. The stability of optimized bimetallic catalysts was also evaluated by recycling tests.

2. Results and Discussion

2.1. Characterization Results

The XRD patterns for calcined and reduced samples of monometal (Ni, Cu) and bimetal Ni-Cu (total metal loading fixed at 20 wt.% with varied relative Ni and Cu loading) on m-SiO_2 are illustrated in Figure S1 from Supplementary Materials and Figure 1, respectively. For the calcined samples, all samples show a broad peak at 22°, which is attributed to the amorphous silica (JCPDS 29-0085) [29]. A significant difference is observed

in monometallic and bimetallic catalysts on m-SiO_2 in different loadings of Ni and Cu by direct alkaline hydrothermal method. The XRD profile of Ni_{20} on m-SiO_2 did not show any peak corresponding to the NiO phase (JCPDS 04-0835). As for the XRD patterns of Cu_{20}/m-SiO_2 catalyst exhibit peaks at 2θ values of 35.5° and 38.8°, which correspond to the monoclinic CuO lattice plane (JCPDS 48-1548) [30]. The crystalline phase evolution of reduced Ni_xCu_y/m-SiO_2 (Figure 1) shows CuO appears nearly fully reduced to metallic Cu, exhibiting peaks in 2θ values of 43.6° and 50.6° (JCPDS 04-0836). In the bimetallic catalysts, the metallic Cu shifted towards a higher 2θ value than the Cu_{20}/m-SiO_2; the shift is indicative of the formation of Ni-Cu alloy on silica support [18]. For comparison, a Ni_5Cu_{15}/C-SiO_2 prepared by wet impregnation on a commercial SiO_2 showed the corresponding XRD pattern in Figure S2, exhibiting various peaks related to metallic Cu (2θ values of 43.6° and 50.6°, JCPDS 04-0836) and Ni (2θ values of 44.6°, JCPDS 04-0850) phases. Compared with wet impregnation, the direct alkaline hydrothermal method produced catalysts with high metal dispersions. According to the XRD results, metallic Cu diffraction peaks are sharper in the monometallic Cu_{20}/m-SiO_2 catalyst than on monometallic Ni_{20}/m-SiO_2 catalyst, indicating that Cu particles are substantially larger. Metallic Ni appears to have strong interaction with SiO_2, generating stable nickel silicates. From the XRD, we did not find the metallic Ni peak in the bimetallic catalysts, which may be due to the smaller size of Ni particles. The average sizes of Cu metal crystallite in mono- and bimetallic catalysts were estimated by following the Scherrer equation as described in Table 1. Hierl et al. [31] reported that in Ni-Cu/Al_2O_3, Ni ions have a strong tendency to occupy subsurface layer and in bulk, causing Cu ion redistribution that is accompanied by enhanced surface segregation of Cu crystallites, and resulting in larger Cu particles. A similar phenomenon appears to exist to account for the increased Cu crystallite size in the Ni_xCu_y/m-SiO_2 samples as compared to the Cu_{20}/m-SiO_2 (Table 1).

Table 1. Chemical and structural properties of Ni_xCu_y/m-silica catalysts.

S.No	Catalysts	Nominal [a] (wt.%)		ICP [b] (wt.%)		Crystallite Size [c] (nm)	
		Ni	Cu	Ni	Cu	Ni	Cu
1	Ni_{20}/m-SiO_2	20	0	-	-	<4	-
2	$Ni_{15}Cu_5$/m-SiO_2	15	5	14.6	4.4	n.d	15.4
3	$Ni_{10}Cu_{10}$/m-SiO_2	10	10	9.2	10.1	n.d	13.08
4	Ni_5Cu_{15}/m-SiO_2	5	15	5.1	14.6	n.d	11.10
5	Cu_{20}/m-SiO_2	0	20	-	-	-	10.70
6	Ni_5Cu_{15}/C-SiO_2	5	15	-	-	7.2	28.80

[a] Nominal loading of copper and nickel metal on silica, [b] metal loading by ICP-OES, and [c] the average crystallite size evaluated by the Scherrer equation: $d_{hkl} = K(\lambda/\beta)\cos\theta$, where K is the structure constant (0.9 for spherical crystals), λ is the incident ray wavelength (0.1541 nm), β is the peak width at half height after correction for instrumental broadening (rad), and θ is the Bragg angle. n.d.: not detected by XRD at a high angle.

Fourier-transform infrared spectroscopy (FTIR) has been used to characterize calcined and reduced Ni_xCu_y on m-SiO_2 catalysts (Figures 2 and S3). The strong absorption band between 3700 cm^{-1} and 3000 cm^{-1} is assigned to the asymmetric OH stretching vibration of water and/or silanol groups [32]. The absorption bands at 467 cm^{-1}, 795 cm^{-1} and 1090 cm^{-1} correspond to symmetric and antisymmetric stretching vibrations of Si-O-Si and bending vibrations of Si−OH [32]. The absorption band at 671 cm^{-1} is assigned to Ni-O-Si in calcined Ni_{20}/m-SiO_2, $Ni_{15}Cu_5$/m-SiO_2, $Ni_{10}Cu_{10}$/m-SiO_2, and Ni_5Cu_{15}/m-SiO_2 [24]. The absorption band at 570 cm^{-1} is attributed to stretching vibrations of Cu−O (Figure S3) [23], indicating the existence of CuO particles in the calcined Ni-$Cu_{0.25}$/m-SiO_2, Ni-$Cu_{0.75}$/m-SiO_2, and Cu/m-SiO_2. In the reduced Ni_xCu_y on m-SiO_2 catalysts (Figure 2), these absorption bands corresponding to Ni-O and Cu-O appear too weak to be observed, consistent with the reduced metallic Ni and Cu. For comparison, FTIR spectra of reduced Ni_5Cu_{15}/C-SiO_2 are shown in Figure 2 (vi). The profiles of silanols are deconvoluted as shown in Figure S4 and the results are summarized in Table S1. The

quantity of monohydrogen-bonded silanols is much higher in Ni_xCu_y/m-SiO_2 than that in Ni_5Cu_{15}/C-SiO_2 [22].

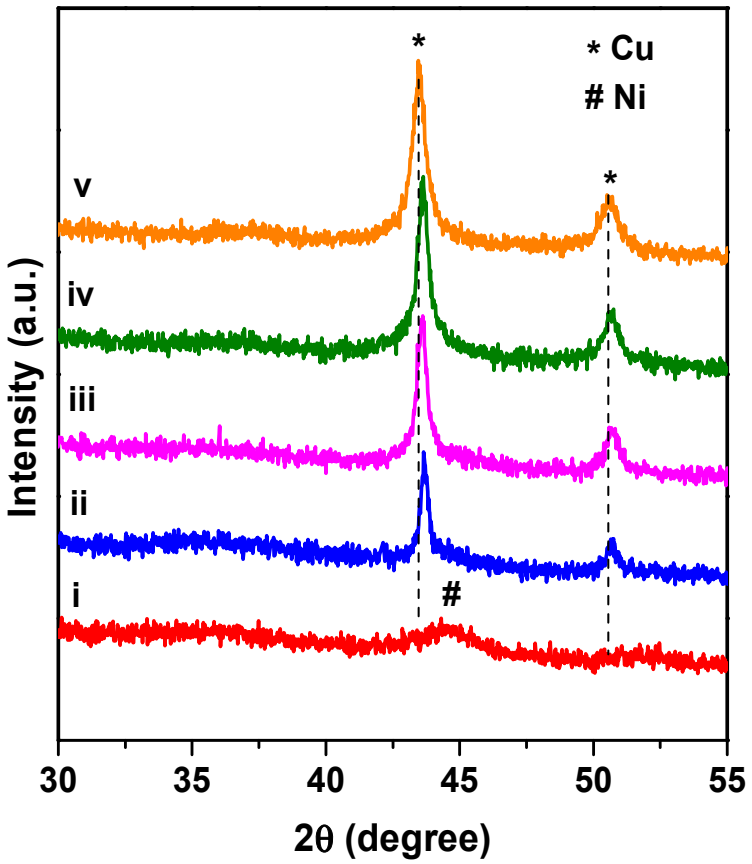

Figure 1. XRD patterns of reduced catalysts (**i**) $Ni_{20}/m-SiO_2$, (**ii**) $Ni_{15}Cu_5/m-SiO_2$, (**iii**) $Ni_{10}Cu_{10}/m-SiO_2$, (**iv**) $Ni_5Cu_{15}/m-SiO_2$, and (**v**) $Cu_{20}/m-SiO_2$ (total metal loading fixed at 20 wt.% with varied relative Ni and Cu loading).

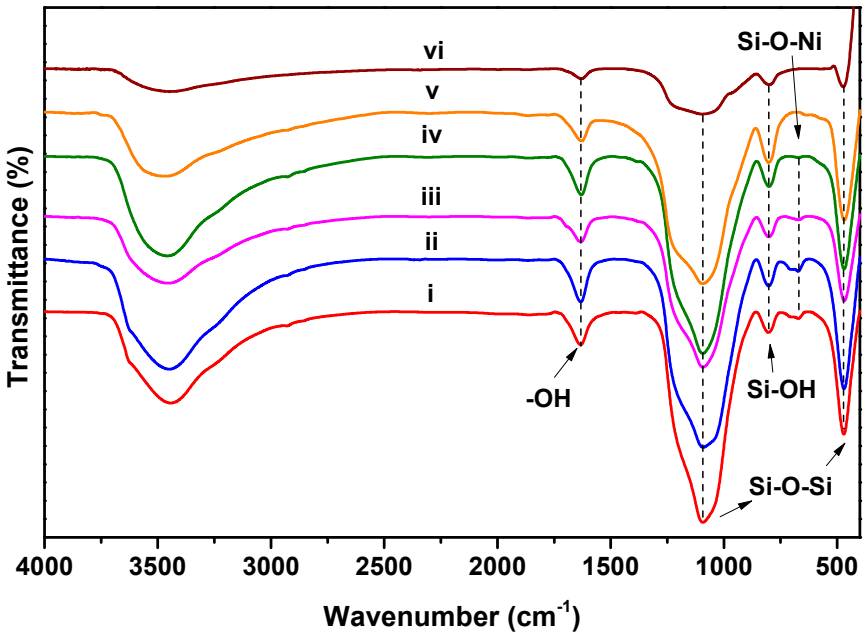

Figure 2. FTIR spectra of reduced catalysts (**i**) $Ni_{20}/m-SiO_2$, (**ii**) $Ni_{15}Cu_5/m-SiO_2$, (**iii**) $Ni_{10}Cu_{10}/m-SiO_2$, (**iv**) $Ni_5Cu_{15}/m-SiO_2$, (**v**) $Cu_{20}/m-SiO_2$, and (**vi**) $Ni_5Cu_{15}/C-SiO_2$.

Temperature-programmed desorption (TPD) of adsorbed NH_3 as a base probing molecule was used to characterize the surface acidity to provide information about strength of acid sites of the Ni_5Cu_{15}/m-SiO_2 and Ni_5Cu_{15}/C-SiO_2 catalysts (Figure S5). The NH_3-TPD profile showed an intense peak above 400 °C, which is attributed to the dehydration of the silanol functional group (Si-O-H) in the silica support [29]. This acidity had no significant impact on the catalytic activity of FAL hydrogenation. Hence, we focused mainly on the strength of acidity from which NH_3 was desorbed below 400 °C. The Ni_5Cu_{15}/m-SiO_2 exhibited a strong desorption peak around 230 °C, but the NH_3 desorption peak was very weak on Ni_5Cu_{15}/C-SiO_2. Lehmann et al. [33] reported that in Ni/MCM-41 a medium NH_3 desorption peak was increased with increasing Ni loading due to the nickel silicate, a similar phenomenon was observed over Fe/MCM-41 [34].

The morphology and metal dispersion on the catalyst were investigated by scanning electron microscopy and energy-dispersive X-ray analysis (SEM-EDX) (Figure 3). Spherical morphology was noticed for all studied samples. It was seen that the three catalysts retained their morphology even after doping with various weight ratios of nickel and copper. Elemental mapping was used to observe the distribution of Ni, Cu, O, and Si particles on the m-SiO_2 (Figure 3, the selected area in pink square box). The homogeneous distribution of Cu, Ni, Si, and O particles on the m-SiO_2 support was noticed. The metal loading was further confirmed by EDX, and the values are summarized in Table 2. The metal content of Ni and Cu from EDX is well matched with the ICP results.

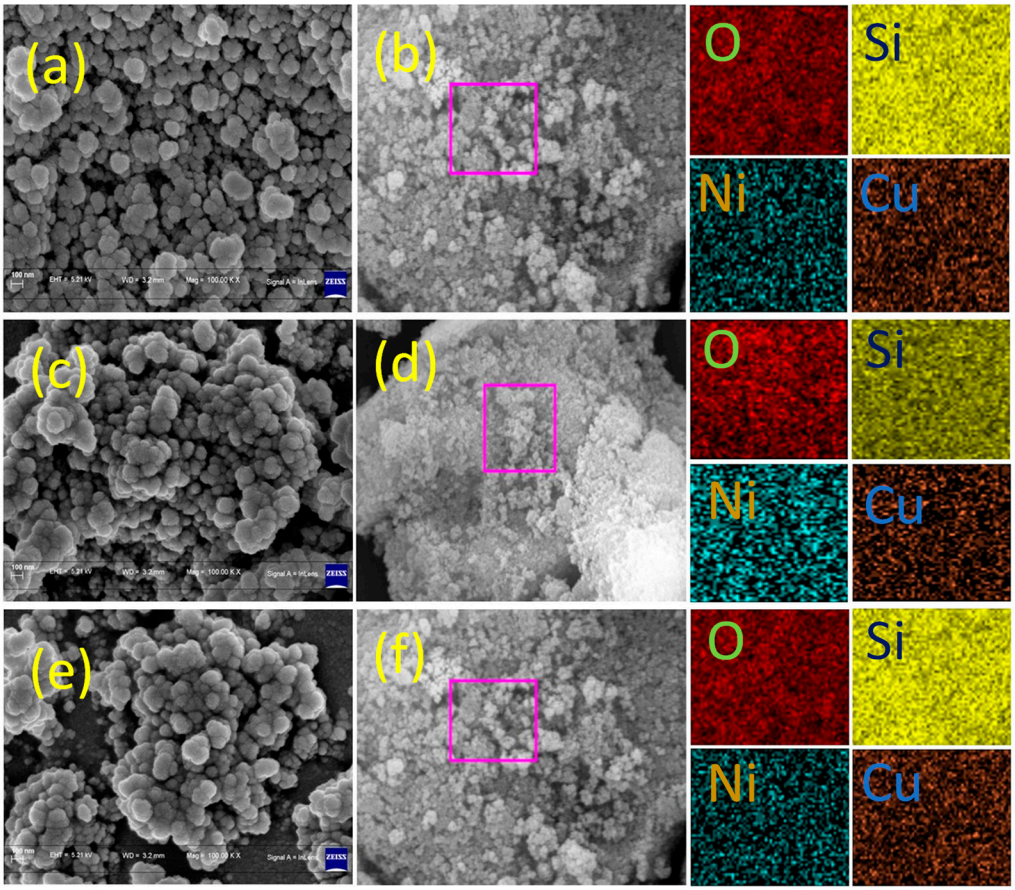

Figure 3. SEM-EDX of $Ni_{15}Cu_5$/m-SiO_2 (**a**,**b**), $Ni_{10}Cu_{10}$/m-SiO_2 (**c**,**d**), Ni_5Cu_{15}/m-SiO_2 (**e**,**f**) catalysts.

Table 2. Physicochemical properties of various amounts of Ni-Cu on SiO_2 support.

S.No	Catalysts	SEM-EDX Ni	SEM-EDX Cu	BET (m^2/g)	V_{pore} (cm^3/g)	D_{pore} (nm)	H_2 Consumption (mmol/g) #
1	m-SiO_2	-		841.2	0.9	3.18	-
2	Ni_{20}/m-SiO_2	-		510.0	0.55	4.57	2.77
3	$Ni_{15}Cu_5$/m-SiO_2	13.4	5.9	496.0	0.77	6.63	4.03
4	$Ni_{10}Cu_{10}$/m-SiO_2	10.0	11.2	567.2	0.74	5.62	3.65
5	Ni_5Cu_{15}/m-SiO_2	4.3	13.5	613.4	0.66	4.59	4.05
6	Cu_{20}/m-SiO_2	-		571.9	0.80	6.07	3.19

Calculated from H_2-TPR.

The morphologies and structural details of the bimetallic Ni and Cu particles in the Ni_5Cu_{15}/m-SiO_2 catalyst was further studied by TEM (Figure 4a). It shows Ni and Cu particles are well dispersed, and the aggregated particles are not observed even after being pretreated at 500 °C. HR-TEM images of Ni_5Cu_{15}/m-SiO_2 sample show particles of ~20 nm and ~5 nm. Figure 4e shows a lattice fringe in the high-resolution HR-TEM images and d-spacing value of ~0.21 nm, corresponding to the (111) plane of the Ni-Cu alloy phase [35].

Hydrogen temperature-programmed reduction (H_2-TPR) was employed to determine the nature of reduction patterns in the synthesized monometallic and bimetallic catalysts as well as the type of reducible species present in the catalysts. The reduction behavior of monometallic and bimetallic Ni_xCu_y on m-SiO_2 catalysts is depicted in Figure 5. For the monometallic Ni_{20}/m-SiO_2 catalyst, a single broad reduction peak in the region of 350–700 °C was observed with T_{max} of 580 °C; this peak was attributed to the reduction of Ni^{2+} in nickel silicate [36]. For the monometallic Cu_{20}/m-SiO_2 catalyst exhibited a reduction peak at 210 °C with a small hump at 170 °C. The H_2 consumption peak at 170 °C and 210 °C are attributed to the reduction of CuO particles dispersed on the m-SiO_2 surface to Cu (I) and the reduction of Cu (I) to Cu (0), respectively [37]. However, all the bimetallic catalysts containing both the metals (Ni and Cu) showed two reduction peaks (190 °C, 550 °C), the low temperature peak is related to the reduction of Cu (ll) to Cu (0) and the high temperature peak is attributed to the reduction of NiO. In the bimetallic catalysts, the Cu reduction peak shifted to a lower reduction temperature than monometallic Cu_{20}/m-SiO_2 catalyst. Hierl et al. [31] reported the influence of Ni on the segregation of Cu from the surface in favor of Ni to occupy subsurface or bulk coordination sites causing the lowering of the reduction temperature for Cu; the nickel silicate facilitated easier reduction of the segregated CuO also accounts for the increased Cu particle size. The presence of Cu in bimetallic catalysts produces spillover hydrogen, which considerably accelerates the nucleation of the Ni metal in these reduction conditions and enhances the reducibility of Ni^{2+} at significantly lower temperatures [38]. The H_2-TPR results are summarized in Table 2.

Figure S6 illustrates the N_2 adsorption and desorption isotherms and the pore size distribution curves of Ni_xCu_y/m-SiO_2 catalysts with various metal ratios. The textural properties of Ni_xCu_y on m–SiO_2 catalysts are summarized in Table 2. The results revealed that all samples exhibited type IV isotherm with an H_2 hysteresis loop, consistent with the mesoporous structure in all the synthesized catalysts [39]. The specific surface area, pore volume, and pore size diameter of the pure m-SiO_2 support are 841 m^2/g, 0.9 cm^3/g, and 3.18 nm, respectively. Compared to the pure m-SiO_2, all the Ni_xCu_y/m-SiO_2 catalysts possessed lower BET surface areas and lesser pore volumes with larger average pore diameters. Sun et al. [22] reported that in FeCo/MCM-41, the partial substitution of silicon ions by iron or cobalt ions in the framework of MCM-41 may inevitably increase pore size and decreased surface area. Notably, when the amount of metals changes on the silica support, the particular surface areas and pore volume changes [40,41].

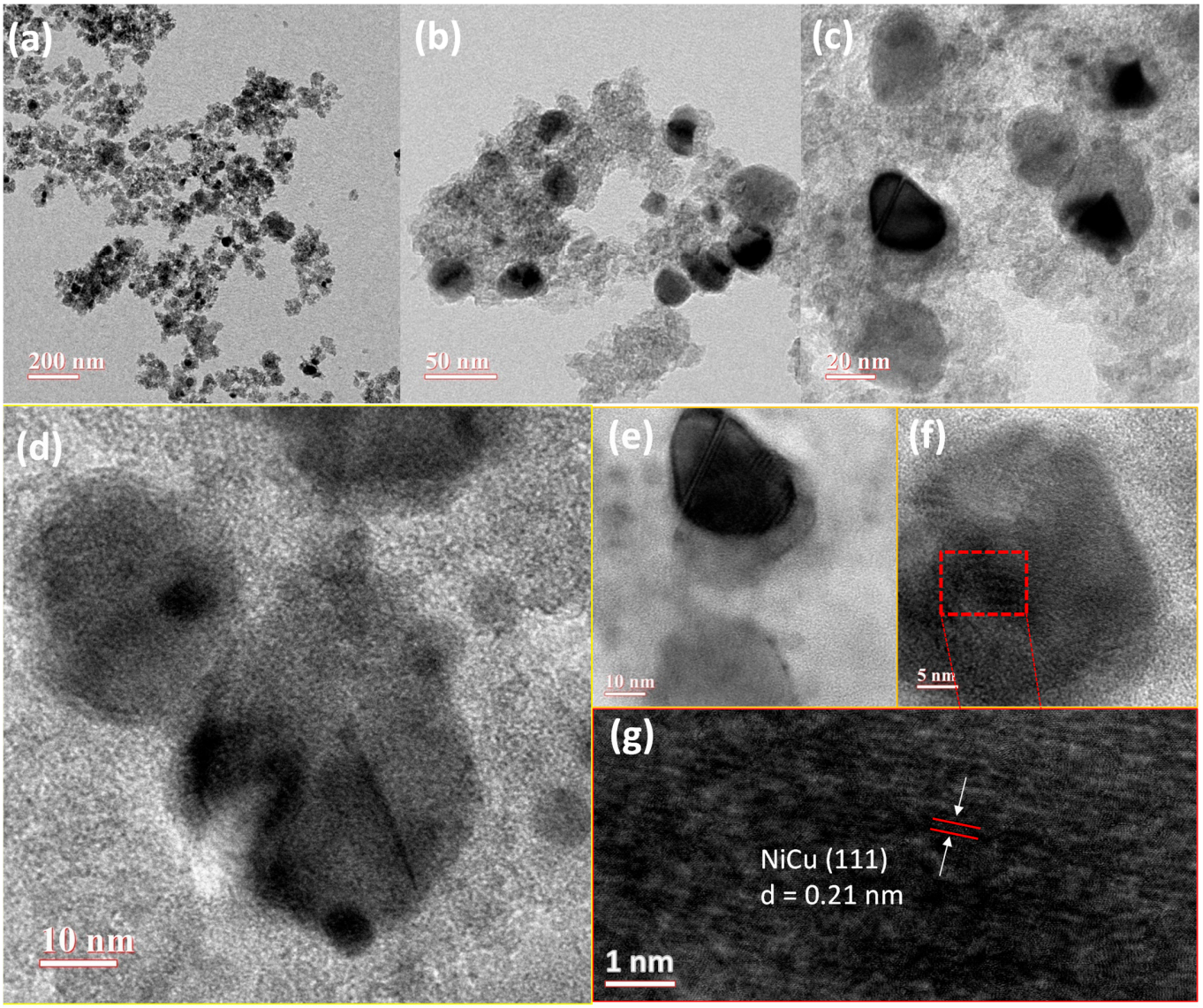

Figure 4. (**a**) TEM image of Ni_5Cu_{15}/m-SiO_2 catalyst; (**b**–**f**) HRTEM image of Ni_5Cu_{15}/m-SiO_2 catalyst; (**g**) Expend view of selected area with red rectangle shape in (**f**).

X-ray photoelectron spectroscopy (XPS) was employed to elucidate the oxidation state, surface composition, and interaction between Cu and Ni of Ni_5Cu_{15}/m-SiO_2 reduced catalyst. The Ni $2p_{3/2}$ core level spectra in Figure 6a showed binding energy (BE) at 855.9 eV attributed to Ni^{2+} in nickel silicates [42]. The appearance of Ni^{2+} in the XPS profile because nickel silicates may not be fully reduced. The XPS spectra of Cu 2p (Figure 6b) showed two main peaks located at 933.5 eV and 935.8 eV, attributed to the presence of Cu^0/Cu^{1+} and Cu^{2+} species, respectively [43]. The BE at 933.5 eV is due to the alteration in unfilled-band electron holes arising during the charge transfer of the strong electron donor species from Cu to the adjacent Ni. This result contributed to the stronger electronic interaction between the bimetallic Ni-Cu [43]. In XPS spectrum of O 1s, three main peaks at 530.9 eV, 533.0 eV, and 535.2 eV correspond to Ni-O/Cu-O, Si-O-Si, and Si-OH, respectively [44]. XPS spectra of Si 2p shows two peaks at 103.7 eV and 105.3 eV, which are assigned to O-Si-O and Si-OH, respectively [45].

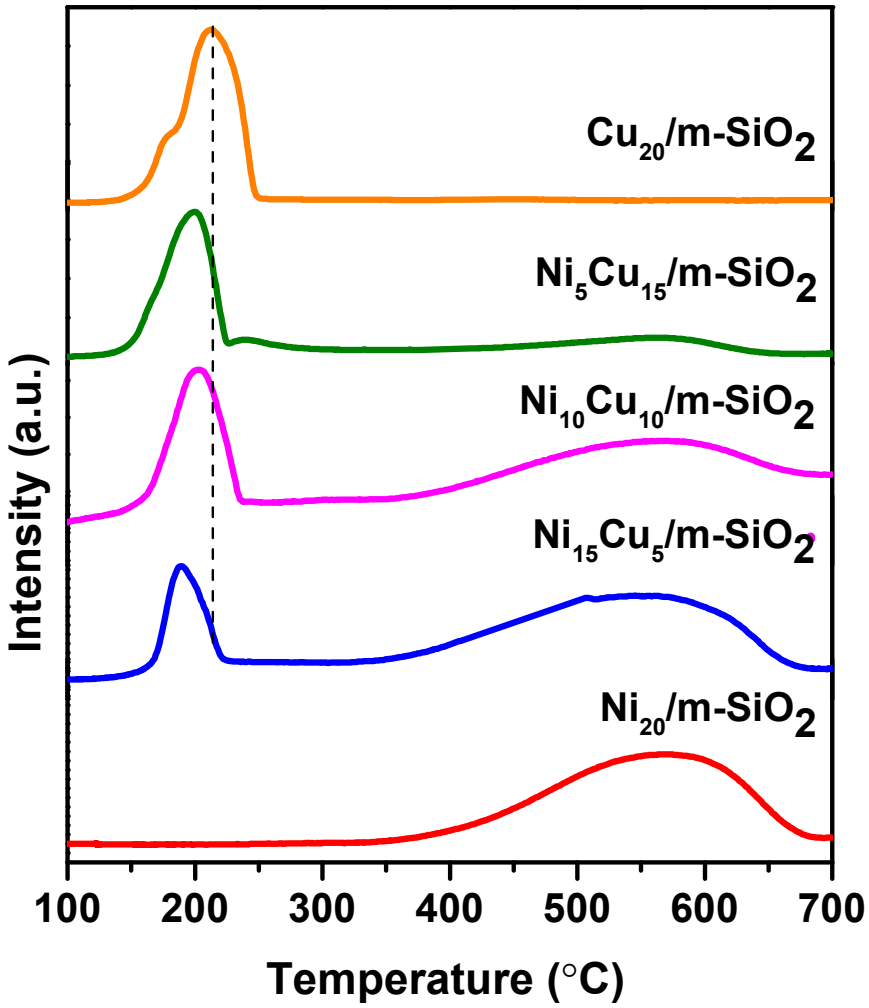

Figure 5. H_2-TPR profiles of Ni_xCu_y/m-SiO_2 catalysts.

2.2. Catalytic Activity

Catalytic hydrogenation of furfural (FAL) to cyclopentanone (CPO) involves several reaction steps, including hydrogenation of FAL to FOL, further ring-rearrangement to 4-hydroxy-2-cyclopentenone (4-HCP) and final dehydration/hydrogenation of 4-HCP to CPO. Metal/acid bifunctional catalysts are favorable for the conversion of FAL to CPO because the metal can accelerate the hydrogenation, and acidic sites promote the ring-rearrangement of FOL through H^+ ions. The Ni_xCu_y/m-SiO_2 catalysts prepared by the direct alkaline hydrothermal method were evaluated for this reaction under the optimized reaction conditions of 3 MPa H_2 pressure and 140 °C temperature. The conversion of furfural and product distributions are presented in Figure 7. On these catalysts, CPO and CPL were formed with different distributions. Ni_{20}/m-SiO_2 catalyst showed 42% FAL conversion with 43% CPO selectivity. While Cu_{20}/m-SiO_2 catalyst showed 53% FAL conversion with 37% selectivity of CPO [16]. Compared to monometallic catalysts, all bimetallic catalysts showed almost 99.9% FAL conversion due to the formation of Ni-Cu alloy on the mesoporous silica support. By increasing Cu composition in the bimetallic catalyst, the selectivity of CPO was gradually increased and reached a maximum of 89.6% with Ni_5Cu_{15}/m-SiO_2 composition. In contrast, Ni_5Cu_{15}/C-SiO_2 shows 76% conversion of FAL with selectivity of 62.1%, 16.3%, and 10.4% to CPO, FOL, and THFA, respectively. While Ni-Cu alloy can form on both catalysts. The higher selectivity of CPO in Ni_5Cu_{15}/m-SiO_2 than in Ni_5Cu_{15}/C-SiO_2 may be ascribed to the much higher quantity of monohydrogen-bonded silanol groups (Figure S4), which is beneficial for ring rearrangement reaction. According to Heitmann et al. [46], monohydrogen-bonded silanols are more active in the

Beckmann rearrangement of cyclohexanone oxime. A similar phenomenon was observed in intermediate FOL rearrangement. The reaction was carried out at low conversions of FAL, as shown in Figure S7, which indicates FOL is a primary product of FAL hydrogenation on the Ni_5Cu_{15}/m-SiO_2 catalyst.

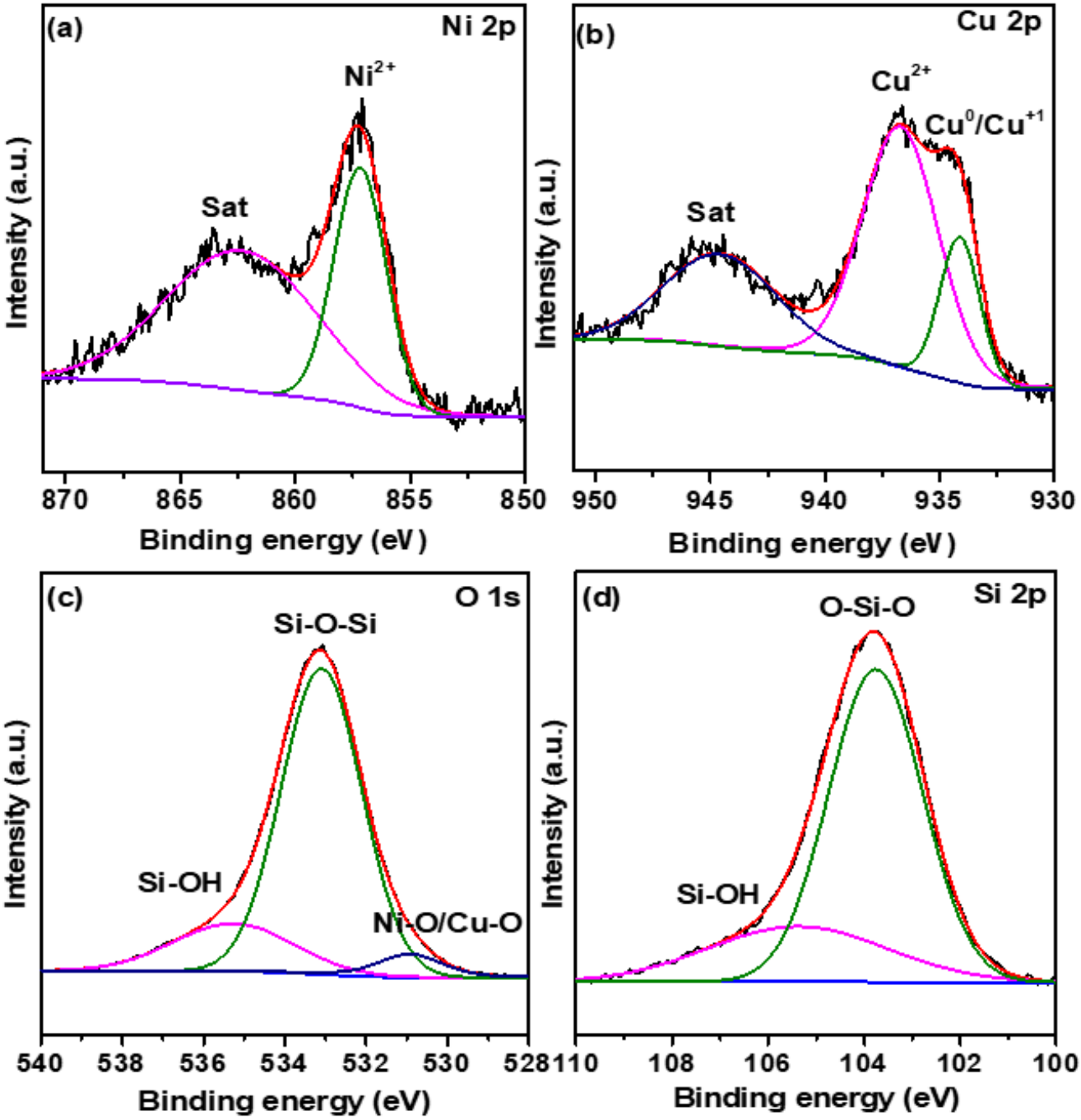

Figure 6. XPS spectra of (**a**) Ni-2p, (**b**) Cu-2p, (**c**) O-1s, and (**d**) Si-2p in the ex situ reduced Ni_5Cu_{15}/m-SiO_2 catalyst.

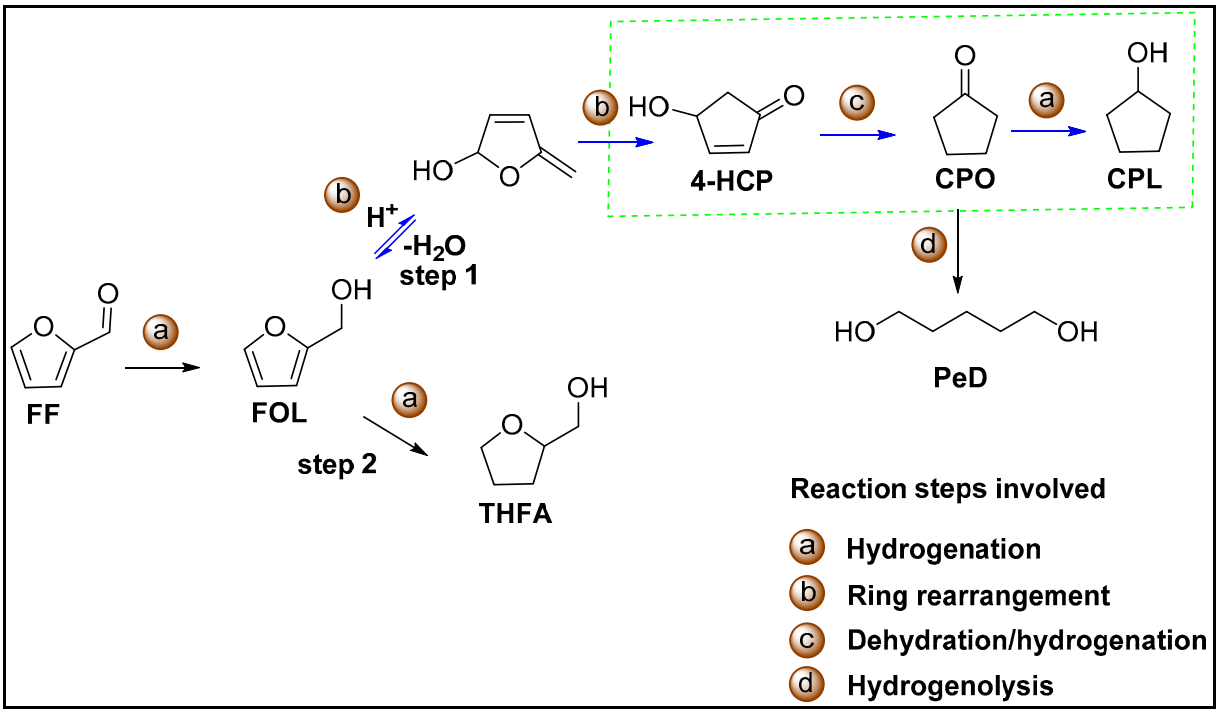

Scheme 1. Possible reaction pathway of hydrogenation of FAL to CPO over various Ni and Cu supported on m−SiO_2.

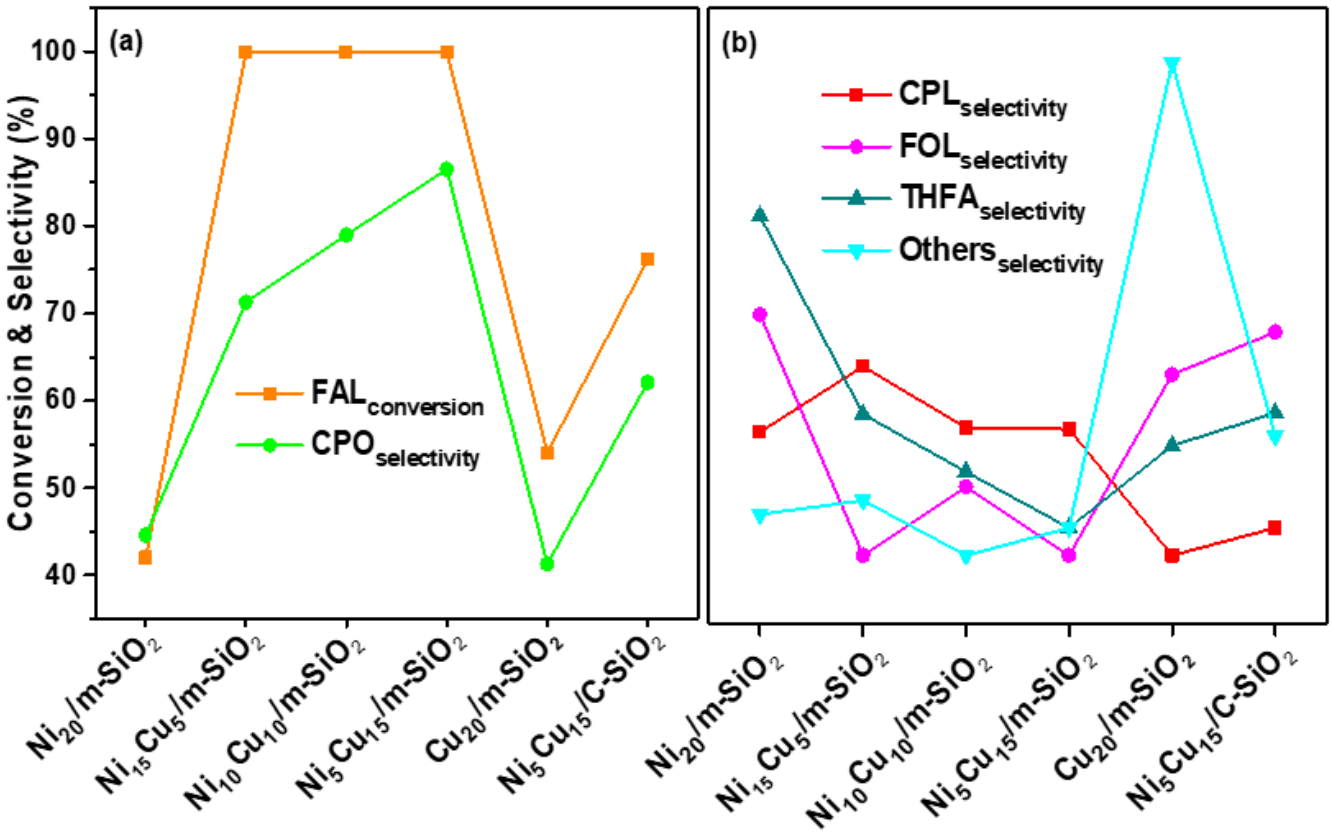

Figure 7. Catalytic performance in furfural (FAL) hydrogenation over metals supported on m-SiO_2. Reaction condition: 5.2 mmol FAL, 15 mL water, catalyst 0.17 g, 140 °C, 3 MPa H_2, 4 h and. See Scheme 1 for product details. (**a**) Conversion of FAL & Selectivity of CPO, (**b**) Selectivity of other products.

The experimental results clearly indicate that the mass ratio of Cu and Ni significantly affects the catalyst's reactivity. The productivity of CPO for optimized Ni_5Cu_{15}/m-SiO_2 catalyst is 7.5 mmol $g_{cat}{}^{-1}$ h^{-1}, which is higher than the reported Ni-Cu based and other catalysts [15,17,18]. The high CPO productivity on Ni_5Cu_{15}/m-SiO_2 catalyst may be due to the appropriate metal mass ratio to form Ni-Cu alloy for selective formation of FOL and further rearrangement of FOL through Brønsted acid sites. Further, it is confirmed through Figure S8 that in the absence of a catalyst, FOL was transformed into 4-HCP without the formation of CPO. The conversion of FOL to 4-HCP should occur by ring opening and closure following a Piancatelli-type rearrangement. In the presence of the catalyst, the FOL conversion and 4-HCP formation increased over Ni_5Cu_{15}/m-SiO_2 and Ni_5Cu_{15}/C-SiO_2, and high conversion was achieved over Ni_5Cu_{15}/m-SiO_2 because of higher surface density of silanol groups on the catalyst surface as indicated by XPS and FTIR analysis. The Ni_xCu_y/m-SiO_2 catalysts synthesized by the direct alkaline hydrothermal method advantageously carry high density of silanol groups for this reaction. The interaction of the silanol groups with water caused the facile production of hydronium ions [22], which is helpful for the rearrangement of FOL. This Ni_5Cu_{15}/m-SiO_2 catalyst was used to optimize the reaction conditions, such as reaction temperature and time.

The effect of reaction temperature on the product distribution for the hydrogenation of FAL over the Ni_5Cu_{15}/m-SiO_2 catalyst is shown in Figure 8a. The major products were FOL, CPO, CPL, and THFA. The conversion of FAL to CPO involves several steps and the details are displayed in Scheme 1. The total selectivity to CPO and CPL is increased with the rising temperature, from 120 °C to 140 °C. The hydronium ions play a key role in the protonation of FOL, which is a key step in the rearrangement of FOL [47]. The selectivity of CPO decreased at 160 °C, while the selectivity of CPL increased when the temperature increased, and traces of diols were observed, due to the over-hydrogenation of CPO [48]. Figure 8b exhibited the effect of reaction time on the FAL conversion and product distribution over Ni_5Cu_{15}/m-SiO_2 at constant temperature (140 °C) and pressure (3 MPa). The FAL conversion was 56.3% with 53.9% selectivity of FOL and 37.8% of CPO formed initially. The highest CPO selectivity to 89.6% was obtained at 4 h of reaction time, and over-hydrogenation of CPO occurred after 4 h. The intermediate product of FOL decreased from 57.8% to <1% with reaction time from 1 h to 4 h. When the reaction time was extended to 5 h, the selectivity of CPO decreased to 82.1% and the selectivity of CPL increased to 11.6%. However, the total yield of CPO and CPL was almost the same when the reaction time reached 5 h, indicating that CPL was mainly obtained from the over-hydrogenation of CPO. According to FAL conversion and CPO yield, a reaction time of around 4 h is optimum for this reaction.

To determine the durability of the synthesized Ni_5Cu_{15}/m-SiO_2 catalyst, multiple tests of used catalyst were carried out for the hydrogenation of FAL to CPO, and the results are shown in Figure 9a. The catalyst was separated after the reaction by centrifugation and washed five times with 2 mL mixture of water/ethanol (1:1 ratio), followed by calcination and reduction to evaluate for the next cycle. Interestingly, the catalyst showed no loss in catalytic activity even after five successive cycles, indicating that the Ni_5Cu_{15}/m-SiO_2 catalyst is stable for FAL conversion to CPO. Figure 9b depicts the leaching test for FAL hydrogenation using the Ni_5Cu_{15}/m-SiO_2 catalyst. With increased reaction time, the FAL conversion increased to 99.9% during 3 h of reaction time. The furfural conversion remains unchanged as the reaction time is extended. The catalyst was removed by centrifugation at 1.5 h of the fifth recycling test. Figure 9b revealed that the FAL hydrogenation was stopped after removing the catalyst. The results also demonstrate that there is no leaching of active species from the solid catalyst even after five successive cycles. This is further confirmed by XRD (Figure S9) and ICP. The ICP analysis showed negligible leaching of Ni and Cu (5.1 wt.% of Ni and 14.6 wt.% of Cu for fresh catalysts, and 4.9 wt.% of Ni and 14.3 wt.% of Cu for spent catalyst) and the CHN analysis determined that the percentage of carbon is around 1.10% after the fifth cycle. These results illustrated that the Ni_5Cu_{15}/m-SiO_2

catalyst is water-tolerant and stable for hydrogenation of FAL to CPO under the optimum reaction conditions.

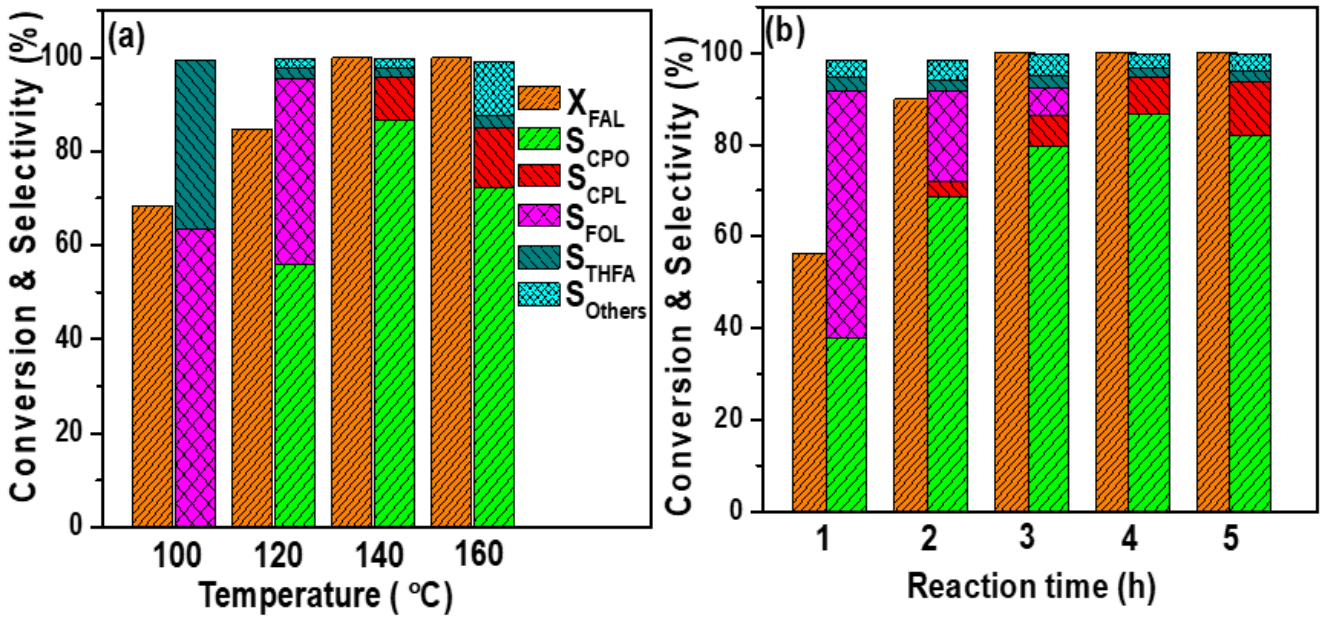

Figure 8. Conversion and selectivity (**a**) at different temperatures for 4 h, and (**b**) with reaction time at 140 °C. Reaction conditions: 0.17 g of Ni_5Cu_{15}/m-SiO_2, 5.2 mmol of furfural, 15 mL of water, 3 MPa of H_2 pressure and X- conversion of FAL, S-selectivity of desired products.

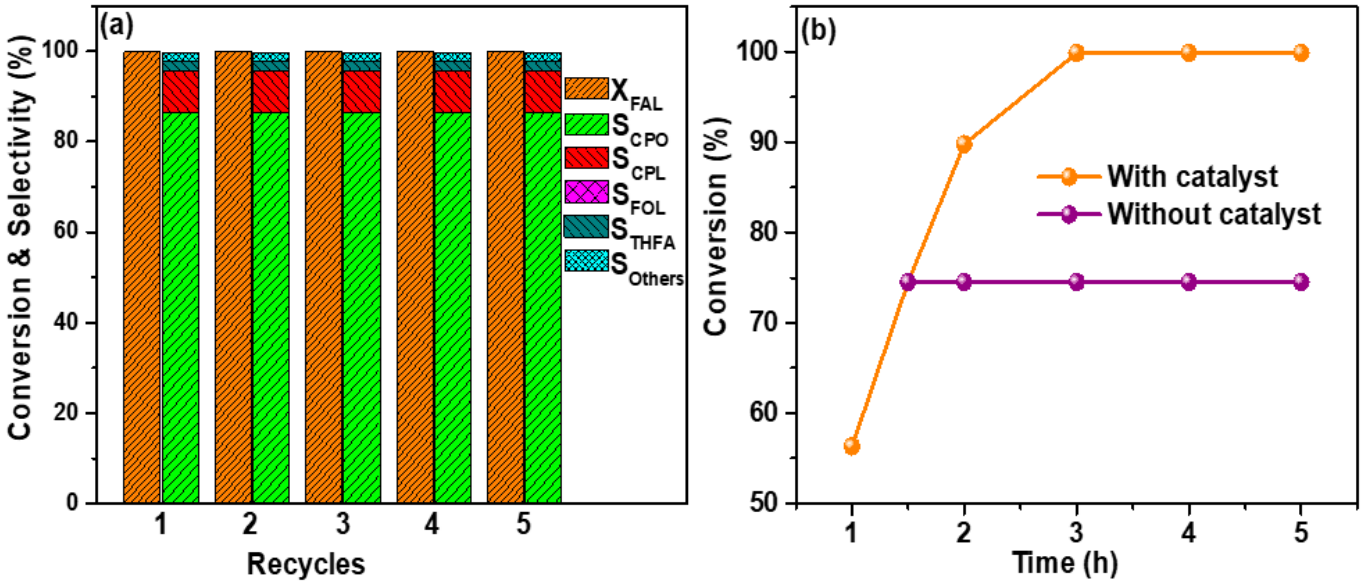

Figure 9. (**a**) Recycled catalyst tests for stability verification of Ni_5Cu_{15}/m-SiO_2 catalyst and (**b**) leaching test for FAL hydrogenation of 5.2 mmol FAL, and 15 mL water, 3 MPa H_2 and X-conversion of FAL, S-selectivity of desired products.

We further examined the reaction pathway of the Ni_5Cu_{15}/m-SiO_2 catalyst for aqueous-phase FAL hydrogenation. In the initial hour of the reaction (Figure 8b), it was found that FOL was a predominant product and then gradually disappeared after 4 h, indicating that FOL may be an intermediate molecule in the conversion of FAL to CPO. CPO yield gradually increases with FOL conversion and reaches its maximum value when the FOL totally disappears. This shows that the intermediate FOL is further transformed into the target product CPO via aqueous-phase Ni-Cu bimetallic catalysis and surface silanols. The reaction that FOL goes through in the aqueous phase into CPO becomes an impediment

to detection due to the very short time and fast rate of the reaction. However, when FOL forms a five-membered carbon ring, the rearrangement reaction is well recognized and water has been found to be a critical solvent in the conversion of FAL to CPO [28]. From the characterization results and catalytic activity, the FAL hydrogenation to CPO proceeds via intermediate FOL. The reaction pathway for the hydrogenation of FAL to CPO in the aqueous phase is depicted in Scheme 1. In this experiment, FAL is hydrogenated to generate FOL before being transformed to CPO (step 1), or THFA (step 2). THFA is formed by total hydrogenation of FOL. At the same time, CPO is formed by FOL rearrangement in water followed by further hydrogenation. CPO selectivity is poor while using the pure Ni_{20}/m-SiO_2 catalyst. After Cu metals are introduced, the Ni-Cu bimetallic catalyst in synergy with the presence of abundant silanol acids cause the preferential rearrangement of the unsaturated structure by under optimal reaction conditions, a significant number of FOL intermediates are rapidly generated by Ni-Cu alloy but at a limited rate of hydrogenation of the C=C bond in the furan ring, the FOL formation is followed by rapid rearrangement by H^+ ions toward CPO formation.

The catalytic activity of the Ni_5Cu_{15}/m-SiO_2 catalyst is compared with the previous reports and summarized in Table 3. The noble metal catalysts (entry 1 and 2) showed good activity. Still, it requires high temperature and pressure to obtain a high CPO yield. Among the non-noble metal catalysts (entries 3–10), the Ni_5Cu_{15}/m-SiO_2 catalyst showed highest CPO yield under optimized reaction conditions. The Cu-Ni-Al-HT catalyst and the Ni-Cu-50/SBA-15 catalyst all showed nearly full FAL conversions. In comparison of over all performances, the Ni_5Cu_{15}/m-SiO_2 catalyst in this work stands out by showing both a high rate in catalytic FAL hydrogenation and CPO yield in relatively milder conditions. Importantly also, the catalyst showed durable performance with little detected leaching of the active metals.

Table 3. Comparison of various catalysts reported in the literature on FAL hydrogenation to CPO.

S.No	Catalysts	Total Metal 10^{-1} (g)	P_{H2} (MPa)	T * (°C) & Time (h)	Rate #	X_{FAL} (%)	Y_{CPO} (%)	Ref.
1	Pt/C	-	8	160 & 0.5	-	99.9	76.5	[10]
2	Au/TiO_2	-	4	160 & 15	-	99.9	99	[12]
3	Ni/SiO_2	0.008	3	160 & 2	3.38	99.9	83.5	[49]
4	Ni-Fe/SBA-15	0.75	3.4	160 & 6	6.25	99.9	90	[14]
5	$10Ni\text{-}10Co/TiO_2$	0.6	4	150 & 4	4.86	99.9	53.3	[15]
6	$15Ni\text{-}10P/Al_2O_3$	0.06	3	150 & 2	4.9	99.9	85.8	[50]
7	Co-Ni/N-CNTs	0.31	0.5	160 & 8	12.5	99.9	95	[51]
8	Cu-Ni-Al-HT	2.25	4	140 & 8	5.2	99.9	95.8	[52]
9	Ni-Cu-50/SBA-15	2	4	160 & 4	11.7	99.9	62	[17]
10	Ni-Cu/Al-MCM-41	0.03	2	160 & 5	16.6	98.3	67.7	[18]
11	Ni_5Cu_{15}/m-SiO_2	0.34	3	140 & 4	15.2	99.9	89.6	pw

*—Temperature, #—the rate of reaction (mmol/g/h), X_{FAL}—FAL conversion, Y_{CPO}—Yield of CPO, Pw-present work.

3. Experimental Study

3.1. Materials and Methods

Furfural was obtained from Avra company limited and was used directly without purification. Tetraethyl orthosilicate (TEOS) was obtained from Sigma Aldrich (Bengaluru, Karnataka, India), cetyltrimethylammonium bromide (CTAB) from SD Fine Chemicals. Nickel nitrate ($Ni(NO_3)_2{\cdot}6H_2O$), cupric nitrate ($Cu(NO_3)_2{\cdot}6H_2O$) of analytical grade, and sodium hydroxide (NaOH) were obtained from Merck. Deionized water in all experiments was purified by a Milli-Q system (Millipore, Mumbai, Maharashtra, India). All other reagents were commercially available.

3.2. Catalyst Preparation

Various wt.% of Ni–Cu/SiO_2 were prepared by the alkaline hydrothermal method [39]. Total metal loading was fixed at 20 wt.% 5 g NaOH was dissolved in 200 mL water with a stirring of 0.25 h, then 4.85 g CTAB was added to the solution for 1 h stirring. Then 27.76 g TEOS and a mixture of various ratios of Cu and Ni precursors in 100 mL solution were simultaneously added to the above solution and agitated for 12 h. The solution was transferred into the Teflon-lined autoclave and kept at 100 °C for 12 h. The resultant solid was cooled, washed with distilled water, and filtered until pH became neutral. The obtained solid was dried overnight and calcined at 550 °C for 4 h with 3 °C/min ramp rate. The monometallic and bimetallic samples were labeled according to their chemical composition as Ni_x/m-SiO_2, Cu_y/m-SiO_2 and Ni_xCu_y/m-SiO_2, where x, y corresponds to weight percentages of Ni and Cu, respectively.

3.3. Catalyst Characterization

The Ni- and Cu-containing samples were analyzed using an Optima 8000 inductively coupled plasma–optical emission spectrometer (ICP-OES) from PerkinElmer, Waltham, MA, USA. The samples were dissolved in mixed nitric acid and hydrofluoric acid.

X-ray diffraction (XRD) patterns of the samples were measured on an X-ray diffractometer (X'Pert powder, PANalytical) from Almelo, Netherlands with a graphite monochromator and Cu-Kα radiation source. The measurements were conducted using the PIXcel 1D detector and operated at 40 kV. The materials were identified by comparing the diffraction data with reference patterns in the database (PDF2-2004).

Fourier-transform infrared spectroscopy (FTIR) measurements of samples were recorded by PerkinElmer 100 FTIR model spectrophotometer by using KBr pellet technique (PerkinElmer, Pune, Maharashtra, India).

Temperature-programmed reduction in hydrogen (H_2-TPR) was performed on a micromeritics AutoChem 2910 chemisorption analyzer (Norcross, GA, USA). For the H_2-TPR experiment, approximately 0.08 g of sample was placed in a tubular quartz reactor. The sample was reduced in 10% H_2/Ar stream by heating from ambient temperature to 700 °C at a heating rate of 10 °C/min. The consumed hydrogen was detected using a thermal conductivity detector (TCD) and quantified using a calibration plot based on quantitative measurement of Ag_2O TPR profiles using a similar protocol.

A field-emission scanning electron microscope (FESEM, JEOL, JSM-7800F, 15 kV, JEOL Ltd., Tokyo, Japan) equipped with an Oxford X-Max silicon drift detector was used to perform EDX analysis.

The catalyst surface area was measured using the commercial BET analyzer (Quantachrome Instrument, Boynton Beach, FL, USA) for N_2 adsorption at −196 °C. Before N_2 adsorption, 0.050 g catalyst sample was degassed under vacuum at 250 °C for 5 h. The textural properties were measured from the nitrogen isotherms using the BET and BJH methods (N_2 adsorption/desorption).

TEM images were taken on a Hitachi HT7700 microscope (M.k, Tokyo, Japan) operated at 100 kV. The sample grid was prepared by ultrasonically dispersed sample in ethanol and deposited droplets of the suspension into a carbon-enhanced copper grid. It was dried under the lamp after the deposition. The high-resolution TEM (HR-TEM) images of the samples were obtained on an FEI-Tecnai G2-20 TWIN microscope operated at 200 kV.

The elemental composition of the ex-situ reduced sample was determined using X-ray photoelectron spectroscopy (Thermo Fisher Model, Madison, WI, USA) with Kα radiation as the exciting source. The binding energies (B.E) were corrected using carbon as a standard reference peak of C 1 s B.E 284.6 eV (B.E calibration). Shirley method of background was used in treating the baseline. The peak fitting of XPS data was done by the Gaussian–Lorentzian fitting function and the proportion was 20:80 (G:L). We used Xpspeak41 software in deconvolution spectra and peak fitting.

CHNSO is the elemental analysis of catalysts. The carbon content of the catalyst after the reaction was determined on a Vario EL cube CHNSO elemental analyzer (Elementar,

Langenselbold, Germany) with a thermal conductivity detector. This instrument is capable of determining the carbon, hydrogen, nitrogen, sulfur, and oxygen contents in the range of 0.01–100% by burning the sample in flowing oxygen at 1170 °C. The time taken by this analysis is approximately 10 min.

3.4. Catalytic Evaluation

The FAL was hydrogenated in a sealed 50 mL stainless steel KBH batch reactor. In a typical process, 5.2 mmol of furfural, 15 mL of water, and 0.17 g of catalyst (pre-reduced at 500 °C for 1 h) were loaded into the reactor at ambient temperature. The reactor was purged 3 times with 0.5 MPa N_2 to remove air and then filled with H_2 up to 3 MPa. The reactor was heated to the operating reaction temperature and kept for the specified reaction time. The reaction mixture was stirred at a rate of 700 rpm. After completion of the reaction, the reactor was cooled to room temperature. The solid catalyst was separated by centrifugation (4000× *g* rpm, 5 min). The reaction mixture was mixed with 5 mL ethanol at room temperature and sonicated for 5 min. The products were identified by gas chromatography–mass spectrometry (GC-MS) (Agilent 7890A-5975C HP-5MS) and quantified by gas chromatography (Agilent 6850), which is equipped with the flame ionization detector (FID) and HP-5 column (30 m × 0.32 mm × 0.25 µm).

The conversion of furfural and the selectivity of the products were calculated using Equations (1) and (2), respectively.

$$\text{FAL conversion } (\%) = \left[1 - \frac{(\text{moles of FAL reactant})_{\text{out}}}{(\text{moles of FAL reactant})_{\text{in}}}\right] \times 100 \quad (1)$$

$$\text{Product selectivity } (\%) = \frac{\text{moles of product}}{(\text{moles of FAL reactant})_{\text{in}} - (\text{moles of FAL reactant})_{\text{out}}} \times 100 \quad (2)$$

4. Conclusions

In this work, monometallic and bimetallic Ni-Cu_x on m-SiO_2 catalysts were synthesized via the alkaline hydrothermal method (in situ preparation) and evaluated for selective hydrogenation of FAL to CPO. Various characterization techniques, including XRD, FTIR, H_2-TPR, HR-TEM, SEM, and XPS, were employed to investigate the formation of Ni-Cu alloy over mesoporous silica. Furthermore, the existence of silanol groups on the catalyst surface was confirmed by XPS and FTIR analysis. The bimetallic catalysts exhibited higher catalytic activity than monometallic catalysts due to the formation of Ni-Cu alloy. The H_2-TPR and HR-TEM results revealed that the addition of Cu species enhances the reduction behavior of Ni species, which improves metal dispersion and active sites for the reaction. Moreover, Ni-Cu alloy plays a prominent role in the adsorption of FAL on the catalyst surface, which prevents the hydrogenation of the C=C bond in the furan ring. This step is crucial for the formation of CPO via selective hydrogenation of C=O to produce a FOL intermediate. It is a further rearrangement to CPO with H^+ ions. The chemical composition of the Ni-Cu and silanol groups in bimetallic catalysts is critical in achieving superior CPO productivity at about 7.5 mmol $g_{cat}{}^{-1}$ h^{-1}.

Supplementary Materials: The following supporting information can be downloaded at: https://www.mdpi.com/article/10.3390/catal13030580/s1, Figure S1: (a) XRD patterns of calcined pure m-SiO_2, and Ni_xCu_y/m-SiO_2 (total metal loading fixed at 20 wt.% with varied relative Ni and Cu loading) and (b) expanded view of XRD patterns in 2θ from 34° to 40°, Figure S2: (a) XRD patterns of reduced Ni_5Cu_{15}/m-SiO_2 and Ni_5Cu_{15}/C-SiO_2 catalysts and (b) expanded view of XRD patterns in 2θ from 42° to 52°, Figure S3: FTIR spectra of calcined (i) pure m-SiO_2, (ii) Ni_{20}/m-SiO_2, (iii) $Ni_{15}Cu_5$/m-SiO_2, (iv) $Ni_{10}Cu_{10}$/m-SiO_2, (v) Ni_5Cu_{15}/m-SiO_2, and (vi) Cu_{20}/m-SiO_2 catalysts, Figure S4: FTIR of reduced catalysts, Figure S5: NH_3-TPD of Ni_5Cu_{15}/m-SiO_2 and Ni_5Cu_{15}/C-SiO_2, Figure S6: BET of silica after metal loading on silica. (a) m-SiO_2, (b) Ni_{20}/m-SiO_2, (c) $Ni_{15}Cu_5$/mSiO_2, (d) $Ni_{10}Cu_{10}$/m-SiO_2, (e) Ni_5Cu_{15}/m-SiO_2, and (f) Cu_{20}/m-SiO_2, Figure S7: Catalytic performance in furfural (FAL) hydrogenation over metals supported on m-SiO_2. Reaction condition: 5.2 mmol FAL, 15 mL water, catalyst 0.05 g, 140 °C, 3 MPa H_2, and 4 h, Figure S8: Rearrangement of furfurylalcohol (FOL) to 4-hydroxy-2-cyclopentenone (4-HCP). Reaction condition: 5.2 mmol FOL, 15 mL

water, reduced catalyst 0.17 g, 140 °C, 3 MPa N_2, 4 h, Figure S9: XRD of Ni_5Cu_{15}/m-SiO_2; Table S1: Characteristic spectra peaks of FTIR [53].

Author Contributions: R.B.: design, data curation, formal analysis, investigation; P.B.: characterization of H_2-TPR, H_2-TPD and XPS; X.Z.: characterization of TEM and HR-TEM, visualization; K.R.: writing draft and NH_3-TPD; H.D.: characterization of XRD and CHNS analysis; S.L.: investigation; V.P.: interpretation of data, writing draft; Z.C.Z.: project administration, supervision, writing—review and editing. All authors have read and agreed to the published version of the manuscript.

Funding: This research was funded by the National Natural Science Foundation of China (grants 21932005 and 22172164), China. We are grateful for the financial support from State Key Laboratory of Catalysis, Dalian Institute of Chemical Physics, Chinese Academy of Sciences.

Data Availability Statement: Data are contained in the article and Supplementary Materials. Any additional data are available on request from the corresponding author.

Conflicts of Interest: The authors declare no conflict of interest related to this work.

References

1. Baral, N.R.; Sundstrom, E.R.; Das, L.; Gladden, J.; Eudes, A.; Mortimer, J.C.; Singer, S.W.; Mukhopadhyay, A.; Scown, C.D. Approaches for More Efficient Biological Conversion of Lignocellulosic Feedstocks to Biofuels and Bioproducts. *ACS Sustain. Chem. Eng.* **2019**, *7*, 9062–9079. [CrossRef]
2. Khemthong, P.; Yimsukanan, C.; Narkkun, T.; Srifa, A.; Witoon, T.; Pongchaiphol, S.; Kiatphuengporn, S.; Faungnawakij, K. Advances in Catalytic Production of Value-Added Biochemicals and Biofuels via Furfural Platform Derived Lignocellulosic Biomass. *Biomass Bioenergy* **2021**, *148*, 106033. [CrossRef]
3. Kalong, M.; Srifa, A.; Hongmanorom, P.; Cholsuk, C.; Klysubun, W.; Ratchahat, S.; Koo-amornpattana, W.; Khemthong, P.; Assabumrungrat, S.; Kawi, S. Catalytic Transfer Hydrogenation of Furfural to Furfuryl Alcohol and 2-Methylfuran over CuFe Catalysts: Ex Situ Observation of Simultaneous Structural Phase Transformation. *Fuel Process. Technol.* **2022**, *231*, 107256. [CrossRef]
4. Putrakumar, B.; Seelam, P.K.; Srinivasarao, G.; Rajan, K.; Rajesh, R.; Ramachandra Rao, K.; Liang, T. High Performance and Sustainable Copper-Modified Hydroxyapatite Catalysts for Catalytic Transfer Hydrogenation of Furfural. *Catalysts* **2020**, *10*, 1045. [CrossRef]
5. Balla, P.; Seelam, P.K.; Balaga, R.; Rajesh, R.; Perupogu, V.; Liang, T.X. Immobilized Highly Dispersed Ni Nanoparticles over Porous Carbon as an Efficient Catalyst for Selective Hydrogenation of Furfural and Levulinic Acid. *J. Environ. Chem. Eng.* **2021**, *9*, 106530. [CrossRef]
6. Renz, M. Ketonization of Carboxylic Acids by Decarboxylation: Mechanism and Scope. *European J. Org. Chem.* **2005**, *2005*, 979–988. [CrossRef]
7. Sudarsanam, P.; Katta, L.; Thrimurthulu, G.; Reddy, B.M. Vapor Phase Synthesis of Cyclopentanone over Nanostructured Ceria-Zirconia Solid Solution Catalysts. *J. Ind. Eng. Chem.* **2013**, *19*, 1517–1524. [CrossRef]
8. Van De Vyver, S.; Román-Leshkov, Y. Emerging Catalytic Processes for the Production of Adipic Acid. *Catal. Sci. Technol.* **2013**, *3*, 1465–1479. [CrossRef]
9. Dutta, S.; Bhat, N.S. Catalytic Transformation of Biomass-Derived Furfurals to Cyclopentanones and Their Derivatives: A Review. *ACS Omega* **2021**, *6*, 35145–35172. [CrossRef]
10. Hronec, M.; Fulajtarová, K. Selective Transformation of Furfural to Cyclopentanone. *Catal. Commun.* **2012**, *24*, 100–104. [CrossRef]
11. Hronec, M.; Fulajtarová, K.; Liptaj, T. Effect of Catalyst and Solvent on the Furan Ring Rearrangement to Cyclopentanone. *Appl. Catal. A Gen.* **2012**, *437–438*, 104–111. [CrossRef]
12. Zhang, G.S.; Zhu, M.M.; Zhang, Q.; Liu, Y.M.; He, H.Y.; Cao, Y. Towards Quantitative and Scalable Transformation of Furfural to Cyclopentanone with Supported Gold Catalysts. *Green Chem.* **2016**, *18*, 2155–2164. [CrossRef]
13. Fang, R.; Liu, H.; Luque, R.; Li, Y. Efficient and Selective Hydrogenation of Biomass-Derived Furfural to Cyclopentanone Using Ru Catalysts. *Green Chem.* **2015**, *17*, 4183–4188. [CrossRef]
14. Jia, P.; Lan, X.; Li, X.; Wang, T. Highly Selective Hydrogenation of Furfural to Cyclopentanone over a NiFe Bimetallic Catalyst in a Methanol/Water Solution with a Solvent Effect. *ACS Sustain. Chem. Eng.* **2019**, *7*, 15221–15229. [CrossRef]
15. Li, Y.; Guo, X.; Liu, D.; Mu, X.; Chen, X.; Shi, Y. Selective Conversion of Furfural to Cyclopentanone or Cyclopentanol Using Co-Ni Catalyst in Water. *Catalysts* **2018**, *8*, 193. [CrossRef]
16. Fan, Z.; Zhang, J.; Wu, D. Highly Efficient NiCu/SiO2 Catalyst Induced by Ni(Cu)-Silica Interaction for Aqueous-Phase Furfural Hydrogenation. *Catal. Lett.* **2022**. [CrossRef]
17. Yang, Y.; Du, Z.; Huang, Y.; Lu, F.; Wang, F.; Gao, J.; Xu, J. Conversion of Furfural into Cyclopentanone over Ni-Cu Bimetallic Catalysts. *Green Chem.* **2013**, *15*, 1932–1940. [CrossRef]
18. Zhang, S.; Ma, H.; Sun, Y.; Liu, X.; Zhang, M.; Luo, Y. Selective Tandem Hydrogenation and Rearrangement of Furfural to Cyclopentanone over CuNi Bimetallic Catalyst in Water. *Chin. J. Catal.* **2021**, *42*, 2216–2224. [CrossRef]

19. Sitthisa, S.; Sooknoi, T.; Ma, Y.; Balbuena, P.B.; Resasco, D.E. Kinetics and Mechanism of Hydrogenation of Furfural on Cu/SiO_2 Catalysts. *J. Catal.* **2011**, *277*, 1–13. [CrossRef]
20. Wang, Z.; Jiang, Y.; Zhang, Y.; Shi, J.; Stampfl, C.; Hunger, M.; Huang, J. Identification of Vicinal Silanols and Promotion of Their Formation on MCM-41 via Ultrasonic Assisted One-Step Room-Temperature Synthesis for Beckmann Rearrangement. *Ind. Eng. Chem. Res.* **2018**, *57*, 5550–5557. [CrossRef]
21. Niu, P.; Xi, H.; Ren, J.; Lin, M.; Wang, Q.; Jia, L.; Hou, B.; Li, D. High Selectivity for N-Dodecane Hydroisomerization over Highly Siliceous ZSM-22 with Low Pt Loading. *Catal. Sci. Technol.* **2017**, *7*, 5055–5068. [CrossRef]
22. Sun, X.; Xu, D.; Dai, P.; Liu, X.; Tan, F.; Guo, Q. Efficient Degradation of Methyl Orange in Water via Both Radical and Non-Radical Pathways Using Fe-Co Bimetal-Doped MCM-41 as Peroxymonosulfate Activator. *Chem. Eng. J.* **2020**, *402*, 125881. [CrossRef]
23. Bouchikhi, N.; Adjdir, M.; Bendeddouche, C.K.; Ramdani, A.; Guezzen, B.; Tabti, H.A.; Lakhache, E.M.; Chami, N. The Influence of the Incorporation Method and Mass Ratio of Copper on the Antibacterial Activity of MCM-41. *Silicon* **2021**, *13*, 4473–4480. [CrossRef]
24. Qin, J.; Li, B.; Zhang, W.; Lv, W.; Han, C.; Liu, J. Synthesis, Characterization and Catalytic Performance of Well-Ordered Mesoporous Ni-MCM-41 with High Nickel Content. *Microporous Mesoporous Mater.* **2015**, *208*, 181–187. [CrossRef]
25. Liu, D.; Quek, X.Y.; Cheo, W.N.E.; Lau, R.; Borgna, A.; Yang, Y. MCM-41 Supported Nickel-Based Bimetallic Catalysts with Superior Stability during Carbon Dioxide Reforming of Methane: Effect of Strong Metal-Support Interaction. *J. Catal.* **2009**, *266*, 380–390. [CrossRef]
26. Li, Y.; Wang, J.; Ding, C.; Ma, L.; Xue, Y.; Guo, J.; Wang, S.; Meng, Y.; Zhang, K.; Liu, P. Effect of Cobalt Addition on the Structure and Properties of Ni-MCM-41 for the Partial Oxidation of Methane to Syngas. *RSC Adv.* **2019**, *9*, 25508–25517. [CrossRef] [PubMed]
27. Wang, C.; Tian, Y.; Wu, R.; Li, H.; Yao, B.; Zhao, Y.; Xiao, T. Bimetallic Synergy Effects of Phyllosilicate-Derived NiCu@SiO_2 Catalysts for 1,4-Butynediol Direct Hydrogenation to 1,4-Butanediol. *ChemCatChem* **2019**, *11*, 4777–4787. [CrossRef]
28. Balaga, R.; Ramineni, K.; Zhang, X.; Yan, P.; Marri, M.R.; Perupogu, V.; Zhang, Z.C. Spillover Hydrogen on Electron-Rich Ni/m-TiO2 for Hydrogenation of Furfural to Tetrahydrofurfuryl Alcohol. *Catalysts* **2022**, *12*, 1286. [CrossRef]
29. Balaga, R.; Yan, P.; Ramineni, K.; Du, H.; Xia, Z.; Marri, M.R.; Zhang, Z.C. The Role and Performance of Isolated Zirconia Sites on Mesoporous Silica for Aldol Condensation of Furfural with Acetone. *Appl. Catal. A Gen.* **2022**, *648*, 118901. [CrossRef]
30. Putrakumar, B.; Seelam, P.K.; Srinivasarao, G.; Rajan, K.; Harishekar, M.; Riitta, K.; Liang, T.X. A Comparison of Structure–Activity of Cu-Modified Over Different Mesoporous Silica Supports for Catalytic Conversion of Levulinic Acid. *Waste Biomass Valorization* **2022**, *13*, 67–79. [CrossRef]
31. Hierl, R.; Knözinger, H.; Urbach, H.P. Surface Properties and Reduction Behavior of Calcined CuO Al_2O_3 and CuO-NiO Al_2O_3 Catalysts. *J. Catal.* **1981**, *69*, 475–486. [CrossRef]
32. Van Der Meer, J.; Bardez-Giboire, I.; Mercier, C.; Revel, B.; Davidson, A.; Denoyel, R. Mechanism of Metal Oxide Nanoparticle Loading in SBA-15 by the Double Solvent Technique. *J. Phys. Chem. C* **2010**, *114*, 3507–3515. [CrossRef]
33. Lehmann, T.; Wolff, T.; Hamel, C.; Veit, P.; Garke, B.; Seidel-Morgenstern, A. Physico-Chemical Characterization of Ni/MCM-41 Synthesized by a Template Ion Exchange Approach. *Microporous Mesoporous Mater.* **2012**, *151*, 113–125. [CrossRef]
34. Wang, Y.; Zhang, Q.; Shishido, T.; Takehira, K. Characterizations of Iron-Containing MCM-41 and Its Catalytic Properties in Epoxidation of Styrene with Hydrogen Peroxide. *J. Catal.* **2002**, *209*, 186–196. [CrossRef]
35. Pendem, S.; Mondal, I.; Shrotri, A.; Rao, B.S.; Lingaiah, N.; Mondal, J. Unraveling the Structural Properties and Reactivity Trends of Cu-Ni Bimetallic Nanoalloy Catalysts for Biomass-Derived Levulinic Acid Hydrogenation. *Sustain. Energy Fuels* **2018**, *2*, 1516–1529. [CrossRef]
36. Weerachawanasak, P.; Krawmanee, P.; Inkamhaeng, W.; Cadete Santos Aires, F.J.; Sooknoi, T.; Panpranot, J. Development of Bimetallic Ni-Cu/SiO_2 Catalysts for Liquid Phase Selective Hydrogenation of Furfural to Furfuryl Alcohol. *Catal. Commun.* **2021**, *149*, 106221. [CrossRef]
37. Singh, G.; Khan, T.S.; Samanta, C.; Bal, R.; Bordoloi, A. Single-Step Synthesis of 2-Pentanone from Furfural over Cu–Ni @SBA-15. *Biomass Bioenergy* **2022**, *156*, 106321. [CrossRef]
38. Zelin, J.; Regenhardt, S.A.; Meyer, C.I.; Duarte, H.A.; Sebastian, V.; Marchi, A.J. Selective Aqueous-Phase Hydrogenation of D-Fructose into D-Mannitol Using a Highly Efficient and Reusable Cu-Ni/SiO_2 Catalyst. *Chem. Eng. Sci.* **2019**, *206*, 315–326. [CrossRef]
39. Gao, B.; Zhang, J.; Yang, J.-H. Bimetallic Cu-Ni/MCM-41 Catalyst for Efficiently Selective Transfer Hydrogenation of Furfural into Furfural Alcohol. *Mol. Catal.* **2022**, *517*, 112065. [CrossRef]
40. Liu, M.; Li, S.; Fan, G.; Yang, L.; Li, F. Hierarchical Flower-like Bimetallic NiCu Catalysts for Catalytic Transfer Hydrogenation of Ethyl Levulinate into γ-Valerolactone. *Ind. Eng. Chem. Res.* **2019**, *58*, 10317–10327. [CrossRef]
41. Rath, D.; Parida, K.M. Copper and Nickel Modified MCM-41 An Efficient Catalyst for Hydrodehalogenation of Chlorobenzene at Room Temperature. *Ind. Eng. Chem. Res.* **2011**, *50*, 2839–2849. [CrossRef]
42. Ungureanu, A.; Dragoi, B.; Chirieac, A.; Ciotonea, C.; Royer, S.; Duprez, D.; Mamede, A.S.; Dumitriu, E. Composition-Dependent Morphostructural Properties of Ni-Cu Oxide Nanoparticles Confined within the Channels of Ordered Mesoporous SBA-15 Silica. *ACS Appl. Mater. Interfaces* **2013**, *5*, 3010–3025. [CrossRef] [PubMed]
43. Ang, M.L.; Miller, J.T.; Cui, Y.; Mo, L.; Kawi, S. Bimetallic Ni-Cu Alloy Nanoparticles Supported on Silica for the Water-Gas Shift Reaction: Activating Surface Hydroxyls: Via Enhanced CO Adsorption. *Catal. Sci. Technol.* **2016**, *6*, 3394–3409. [CrossRef]

44. Yuan, E.; Ni, P.; Xie, J.; Jian, P.; Hou, X.; Hashemi, A.; Bahari, A.; Prusik, K. Structural and Dielectric Characteristic of Povidone–Silica Nanocomposite Films on the Si (n) Substrate. *Appl. Phys. A Mater. Sci. Process.* **2017**, *123*, 15716–15731. [CrossRef]
45. Prusik, K. Tuning Physical Properties of $NiFe_2O_4$ and $NiFe_2O_4$ @SiO_2 Nanoferrites by Thermal Treatment. *Metall. Mater. Trans. A* **2022**, *53*, 1208–1230.
46. Heitmann, G.P.; Dahlhoff, G.; Hölderich, W.F. Catalytically Active Sites for the Beckmann Rearrangement of Cyclohexanone Oxime to ε-Caprolactam. *J. Catal.* **1999**, *186*, 12–19. [CrossRef]
47. Li, X.L.; Deng, J.; Shi, J.; Pan, T.; Yu, C.G.; Xu, H.J.; Fu, Y. Selective Conversion of Furfural to Cyclopentanone or Cyclopentanol Using Different Preparation Methods of Cu-Co Catalysts. *Green Chem.* **2015**, *17*, 1038–1046. [CrossRef]
48. Hronec, M.; Fulajtárova, K.; Mičušik, M. Influence of Furanic Polymers on Selectivity of Furfural Rearrangement to Cyclopentanone. *Appl. Catal. A Gen.* **2013**, *468*, 426–431. [CrossRef]
49. Tian, H.; Gao, G.; Xu, Q.; Gao, Z.; Zhang, S.; Hu, G.; Xu, L.; Hu, X. Facilitating Selective Conversion of Furfural to Cyclopentanone via Reducing Availability of Metallic Nickel Sites. *Mol. Catal.* **2021**, *510*, 111697. [CrossRef]
50. Gao, G.; Shao, Y.; Gao, Y.; Wei, T.; Gao, G.; Zhang, S.; Wang, Y.; Chen, Q.; Hu, X. Synergetic Effects of Hydrogenation and Acidic Sites in Phosphorus-Modified Nickel Catalysts for the Selective Conversion of Furfural to Cyclopentanone. *Catal. Sci. Technol.* **2021**, *11*, 575–593. [CrossRef]
51. Wang, D.; Al-Mamun, M.; Gong, W.; Lv, Y.; Chen, C.; Lin, Y.; Wang, G.; Zhang, H.; Zhao, H. Converting Co^{2+}-Impregnated g-C_3N_4 into N-Doped CNTs-Confined Co Nanoparticles for Efficient Hydrogenation Rearrangement Reactions of Furanic Aldehydes. *Nano Res.* **2021**, *14*, 2846–2852. [CrossRef]
52. Zhu, H.; Zhou, M.; Zeng, Z.; Xiao, G.; Xiao, R. Selective Hydrogenation of Furfural to Cyclopentanone over Cu-Ni-Al Hydrotalcite-Based Catalysts. *Korean J. Chem. Eng.* **2014**, *31*, 593–597. [CrossRef]
53. Hu, N.; Rao, Y.; Sun, S.; Hou, L.; Wu, P.; Fan, S.; Ye, B. Structural Evolution of Silica Gel and Silsesquioxane Using Thermal Curing. *Appl. Spectrosc.* **2016**, *70*, 1328–1338. [CrossRef] [PubMed]